International Journal of Modern Manufacturing Technologies
ISSN 2067–3604, Vol. XIV, No. 2 / 2022
https://doi.org/ 10.54684/ijmmt.2022.14.2.226

OPTIMIZING THE DESIGN OF AN EXPLORATION UNDERWATER VEHICLE USING NUMERICAL ANALYSIS

Adrian Sabau, Mihaela Barhalescu, Remus Zagan

Constanta Maritime University, Faculty of Electromechanics,
104 Mircea cel Batran Street, 900663 Constanta, Romania

Corresponding author: Mihaela Barhalescu, mihaela.barhalescu@cmu-edu.eu

Abstract: When it comes to designing a mini-submarine, the most important questions are what it should look like to achieve the purpose for which it was built and what propulsion force is required to operate it at expected parameters. This paper aims to answer some of these questions using a numerical analysis designed to optimize the body shape using the Ansys CFX software package. The mini-submarine understudy is research one and it is equipped with eight thrusters. The optimization aims to choose an optimal body shape between the frame type which is the simplest, cheapest, easiest to execute and offers easy access to all components, and the closed hull type which is more compact has lower hydrodynamic resistance, but is difficult to execute, is expensive and difficult to access inside for interventions and inspection. The cases of study are incompressible turbulent flow for a complete submerged body, distinguished by the complexity of the form and the conditions under which the computation must be performed. The simulation will be done at several speeds, according to the known power of the thrusters in steady-state conditions. The results will be compared whit measuring data, analyzed, and presented comparatively base on hydrodynamic resistance and speed, but will be discussed the other criteria as well.
Key words: thrust force, drag force, steady-state analysis, turbulent flow, momentum equation, numerical scheme.

1. INTRODUCTION

The The importance of remote-controlled underwater vehicles (ROV) has grown significantly in the marine industry and related fields (offshore, research, surveillance, operation, production, and last but not least entertainment). The world production of ROV has increased but also the requirements of different types of users. When it comes to designing an ROV, the most important challenges are what it should look like to achieve the purpose for which it was built and what propulsion force is required to operate it at expected parameters. Over the years many authors have published results from simulations performed with various simulation software including Ansys CFX and Fluent [1-3]. This paper aims to answer some of these questions using a numerical analysis designed to optimize the ROV body shape using the Ansys CFX software package. The present study analyzed the opportunity to optimize the ROV body shape to reduce the hydrodynamic resistance, increase maneuverability, and reduce execution costs. The mini-submarine understudy is research one for which maneuverability is the most important characteristic and plays a decisive role in service. It is equipped with eight thrusters (T100 produced by Blue Robotic), has symmetry concerning the longitudinal plane, and is controlled and powered by the umbilical cable that connects it to the central control unit assisted by the human operator. The optimization aims to choose an optimal body shape between the frame type which is the simplest, cheapest, easiest to execute and offers easy access to all ROV components, and the closed body type which is more compact has lower hydrodynamic resistance, but is difficult to execute, is expensive and difficult to access inside for interventions and inspection. The cases of study are viscous, incompressible turbulent flow for a complete submerged body, distinguished by the complexity of the form and the conditions under which the computation must be performed. The simulation will be done in all directions and at several speeds, evaluated according to the thrust force, and configuration of the propellers, in steady-state conditions.

2. THEORETICAL APPROACHES

The theoretical model used the Reynolds Averaged Navier-Stokes equations which are mainly the ones frequently used to solve this type of problem [2, 3]. The difference, in that case, is that we use for turbulence modelling the k-ϖ model, Shear Stress Transport (SST) formulation, which is known to have more good results instead of the very common standard, k-ε model.
The system of equations of the model are [4]:

• Continuity equation:

$$\nabla(\rho U) = 0 \qquad (1)$$

• Momentum equation:

$$\frac{\partial}{\partial t}(\rho U) + \nabla \cdot (\rho U \otimes U - \mu_{eff}(\nabla U + (\nabla U)^T)) = -\nabla p'$$

(2)

$$\mu_{eff} = \mu + \mu_t, \qquad p' = p + \frac{2}{3}\rho k \qquad (3)$$

where μ_t is turbulent viscosity, μ_t is turbulent viscosity $p`$ modified pressure, and μ_{eff} effective viscosity

• Transport equation for turbulence model k-ϖ, Shear Stress Transport (SST) formulation:

$$\frac{\partial(\rho k)}{\partial t} + \frac{\partial(\rho k U_j)}{\partial x_j} = \frac{\partial}{\partial x_j}\left[\left(\mu + \frac{\mu_t}{\sigma_k}\right)\frac{\partial k}{\partial x_j}\right] + P_k - \beta' \rho k \omega$$

(4)

$$\frac{\partial(\rho\omega)}{\partial t} + \frac{\partial(\rho U_j \omega)}{\partial x_j} = \frac{\partial}{\partial x_j}\left[\left(\mu + \frac{\mu_t}{\sigma_{\omega 1}}\right)\frac{\partial \omega}{\partial x_j}\right] + (1 - F_1) 2\rho \frac{1}{\sigma_{\omega 2}\omega}\frac{\partial k}{\partial x_j}\frac{\partial \omega}{\partial x_j} + P_\omega - \beta_2 \rho \omega^2$$

(5)

$$\mu_t = \rho\frac{k}{\omega}, \quad \nu_t = \frac{\alpha k}{\max(\alpha\omega S F_2)}, \quad \nu_t = \frac{\mu_t}{\rho}, \qquad (6)$$

$$P_\omega = \left(\frac{\alpha_2}{\nu_t}\right) P_k, \quad \sigma_k = 1.176, \quad \sigma_{\omega 2} = \frac{1}{0.856}, \qquad (7)$$

$$\sigma_{\omega 1} = 2, \quad \alpha_1 = \frac{5}{9} \quad \alpha_2 = 0.44, \quad \beta' = 0.09, \quad \beta = 0.0828,$$

(8)

where P_k, P_ω represents the generation of, turbulence kinetic energy (k), turbulent frequency (ϖ) due to the mean velocity gradients, σ_k, σ_ε are the turbulent Prandtl numbers, and F_1, F_2 is a specific blending function, υ_t is a limiter to the formulation of the eddy-viscosity and S is an invariant measure of the strain rate.

The calculation is done running a steady-state analysis, using a simplex algorithm, whit pressure corrections, and a high-resolution option for advection schemes and turbulence numeric.

3. THE THRUSTER AND PROGRAM SETTINGS

3.1. Thrusters' configuration

Figure 1 shows the optimal positioning of the 8 thrusters (BlueRobotics T100), to obtain maximum manoeuvrability. On the figure, the arrows mark the normal direction, ahead (forward) the opposite direction being for the rotation of the propeller in the opposite direction. Thrusters used are asymmetric for this reason the maximum thrust force developed is F_{ahead} = 23.2 N and F_{astern} = 18.1 N. In this configuration the maximum propulsion forces for ahead - astern, up and down – port (left) – starboard (right) are shown in equations 1-4. For maximizing the manoeuvrability, the shunting thrusters are positioned at an angle of 45 degrees to the longitudinal axis of symmetry. The thrusters are positioned on the frame to influence each other as little as possible.

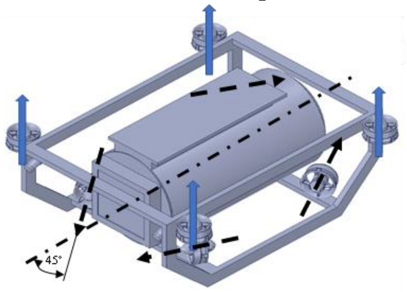

Fig. 1. ROV whit plan front end (PlanF), thrusters' arrangements

The maximum available propulsion force (FP) generated by the propellers is:

$$FP_{\max AHED} = F_{\max ASTERN} = 2 \cdot 22.3\sin(45) + 2 \cdot 18.1\sin(45) = 57.13\,N,$$
$$FP_{\max STARPORT} = F_{\max PORT} = 2 \cdot 22.3\sin(45) + 2 \cdot 18.1\sin(45) = 57.13\,N,$$
$$FP_{\max UP} = 4 \cdot 22.3 = 89.2\,N,$$
$$FP_{\max DOWN} = 4 \cdot 18.1 = 72.4\,N.$$

(9)

3.2. Program settings

The same settings were used for all calculation cases:

• Steady-state analysis;
• Incompressible flow, water, at 1,05 bar;
• k-ϖ turbulent model, Sher Stress Transport formulation;
• Isothermal, water temperature 25ºC;
• Boundary condition (Figure 2):
○ Inlet, normal speed 0.1, 0.25, 0.5, 0.75 and 1 m/s;
○ Outlet Average relative static pressure, 0 bar.
○ Symmetry where is possible ROV have longitudinal symmetry.

Mesh is tetrahedral, whit fine size and smoothing.

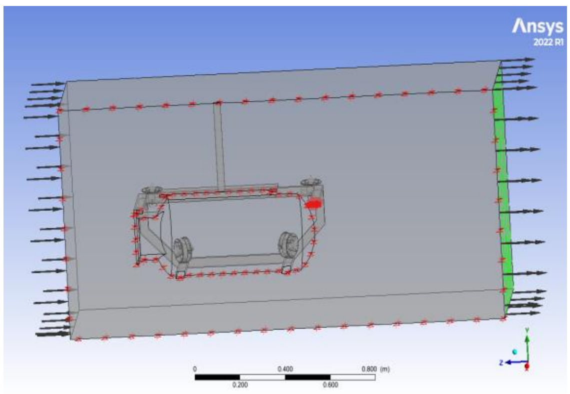

Fig. 2. Program settings

4. MODEL CALIBRATION

The generated model was calibrated using the measurements obtained in the mini hydrodynamic test basin existing in the endowment of the Maritime University. The numerical model was dimensioned according to the dimensions of the hydrodynamic test basin to a 1:1 scale, that has a section of 1 m^2 (1m X 1m) and a working length of 2 m (out of 6 m). The basin has a flow velocity sensor whit transverse displacement that allows the monitoring of the flow velocity variation in the respective section on a rectangle of 200X600 mm from the water surface. For this reason, the entry into the calculation range was positioned at 300 mm in front of the model (flow velocity sensor position), to comply with the basin test configuration and the measured average velocity was introduced in the calculation for a more accurate representation of the concrete test conditions.

The discretization was the biggest problem due to the thrusters that were scanned in 3D, and the resulting geometry had a lot of artifacts that had to be corrected, some of them manually. The repaired mesh was optimized until the results were independent of its fineness, corresponding to a difference of less than 1%. The calibration model is presented in Figure 1, the discretization is shown in Figure 3 and that has 384433 nodes and 2087956 cells. Calculations were made over the entire range of speeds for the ahead direction from 0 to 1 m/s, which could be measured in good condition in the hydrodynamic basin (the basin is small in size). Finally, the generated results were compared with the experimental data. For comparison, we use in simulation two turbulence models, well known for robustness, the k-ω-SST turbulence model and the k-ε Standard model. The most interesting results obtained are shown in Figures 4-9. The figures show the velocity field in the planes of interest (symmetry, vertical, horizontal) represented vectorially, the kinetic pressure as a background contour, and the hydrodynamical resistance (drag force) *DFz*.

Analysing the results presented synthetically in Figure 9 it can be seen that the results are in good agreement with the experimental data (values and allure) and the error is a maximum of 5%. At low speeds the differences are insignificant, but as the speed increases, the errors also increase. Both turbulence models overestimate the hydrodynamic resistance (drag force). The best concordances with the experimental results were obtained by using the k-ω SST model which has better performance, as expected. The maximum ROV speed is less than 1 m / s, from interpolation it would be 0.81 m / s.

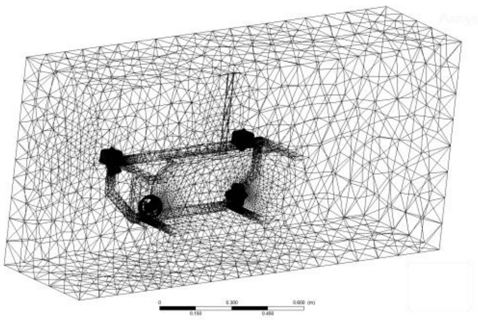

Fig. 3. Mesh

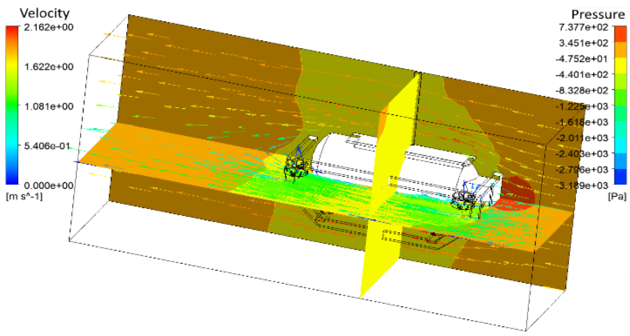

Fig. 4. Pressure, the velocity at v=1 m/s, k-ω SST model, and DFz=-82.342 N

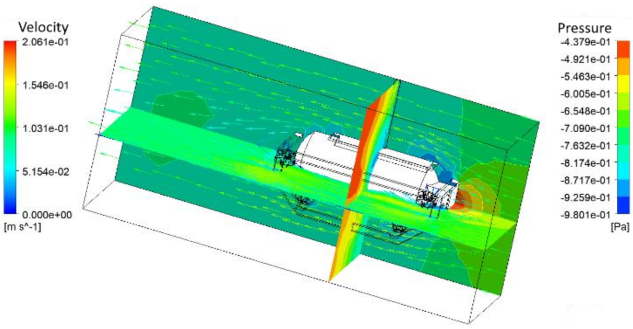

Fig. 5. Pressure, the velocity at v=0.1 m/s, k-ω SST model, and DFz=0.866 N

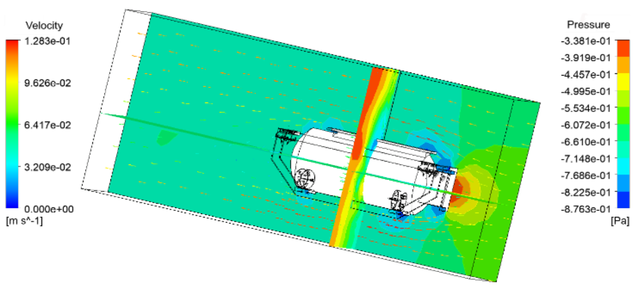

Fig. 6. Pressure, the velocity at v=0.1 m/s, k-ε standard model, and DFz=0.874 N

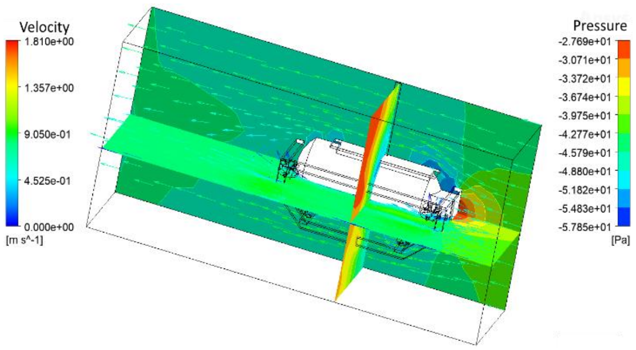

Fig. 7. Pressure, the velocity at v=0.75 m/s, k-ω SST model, and DFz=46.606 N

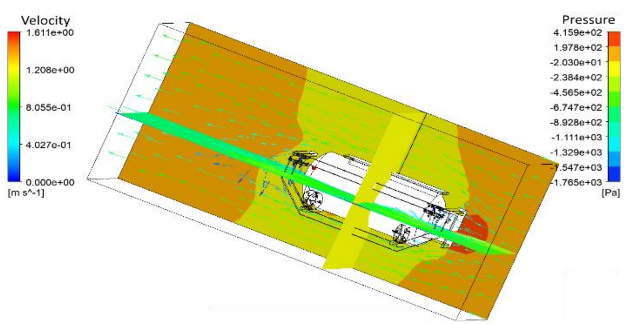

Fig. 8. Pressure, the velocity at v=0.75 m/s, k-ε standard model, and DFz=47.09 N

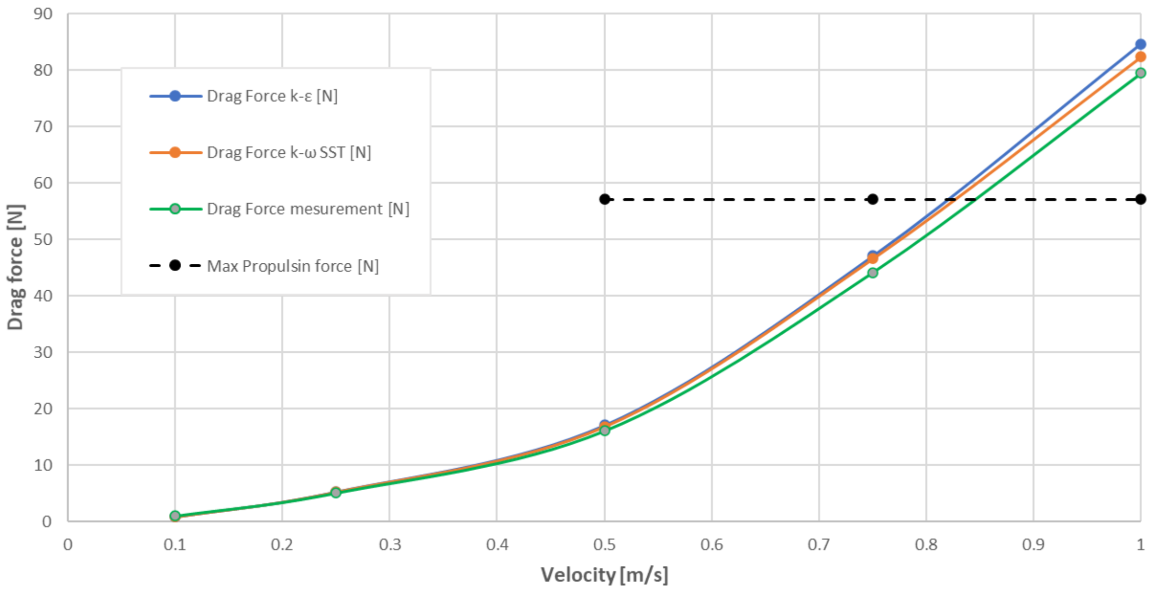

Fig. 9. Drag force versus velocity for measured and calculated data

5. OPTIMIZING ROV DESIGN

The optimization focused on the front of the ROV. The shape of the glazed space at the front of underwater vehicles is of great importance for the quality of acquiring images. After that, the improvement of the nautical qualities is pointed, but also the constructive simplicity and easiest of access to the components for maintenances.

5.1. Optimizing the ROV's front end

Starting from the frame type structure of the ROV, the first optimization aimed at modifying the front end, to improve the nautical qualities but also to increase the sharpness of the images received by the video camera. The easy to execute flat shape (made by the authors) offers distorted images due to water refraction and low viewing angle. From this point of view, the spherical cap is the most suitable but also the most difficult to execute.
Whit these considerations, we did two more tests with the hemicylindrical front area (Figure 10), easier to perform in practice and with a hemispherical shape optimal for the video acquisition part and the viewing angle (Figure 11).
The tests were performed only for ahead movement, this being major influenced by the shape of the frontal area. The simulations were performed under the same conditions as in the previous simulations. The most relevant results are shown in Figures 12-15.
The analysis of the results (Figure 16) as expected confirmed that the hemispherical shape is the most advantageous both from the nautical point of view and for the image acquisition part. The maximum speed can increase by 0.1 m/s from 8.1 m/s (plan front end) to about 0.92 m/s.

5.2. Body optimization

Subsequent optimizations were aimed at improving nautical qualities. As the frame structure cannot offer too many options, closed structures were created. Simulations were performed for three body types, all of which have a hemispherical front end due to these superior performances, even these are more expensive and more complicated to execute:

• Closed body shape that tends to the form of a rotating paraboloid, which has good nautical qualities but is difficult to achieve from a practical point of view and is more unstable in operation;
• Prismatic compact body that is easier to make and has good stability when manoeuvring;
• Composite body, which should be a combination of closed and frame bodies, easier to execute but also have good nautical qualities and additionally remove the main disadvantage of closed bodies, the problem of cooling. The described ROV has inside electrical equipment with an installed power of over 1000 W that dissipates a large amount of heat, which is mandatory to be evacuated.

Using the information obtained in previous simulations, it turned out that to verify the efficiency of the optimization, it is sufficient to test the nautical qualities at a maximum speed that in our case is about 0.75 m/s, in all directions, being mainly the maximum possible operating speed. The simulations will be performed under the same conditions as in the previous simulations. The newly created variants will have the same interior volume as those in the frame structure. The floating space, stabilization weights, and equipment are all embedded inside.

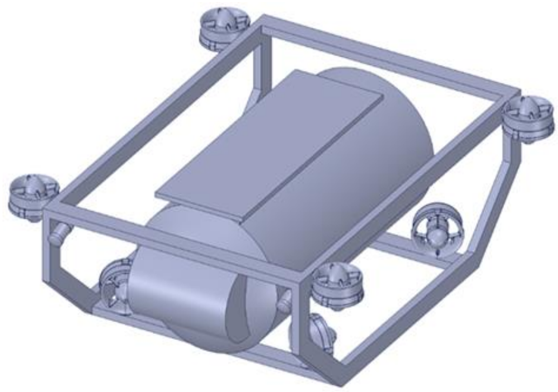

Fig. 10. ROV whit hemicylindrical front end (CyliF)

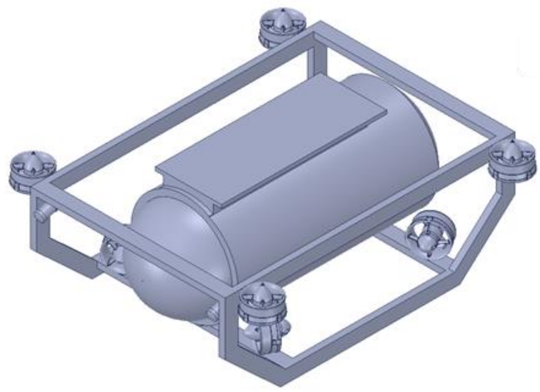

Fig. 11. ROV whit hemispherical front end (SphF)

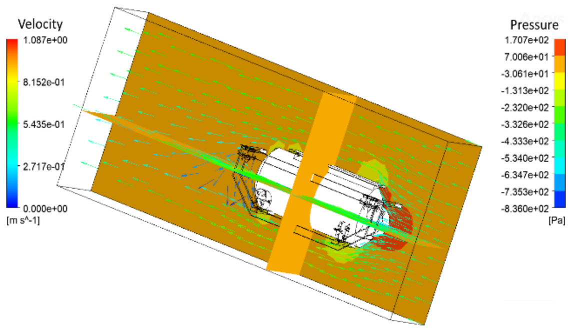

Fig. 12. Hemicylindrical front end at v=0.5 m/s, pressure, velocity, and DFz=16.1 N

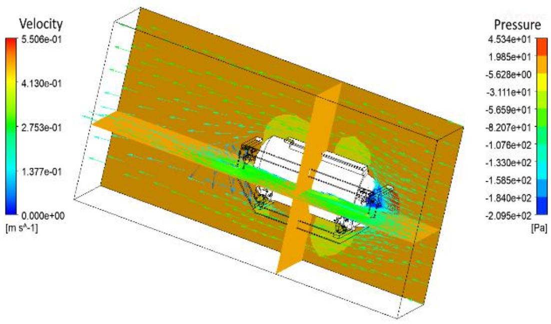

Fig. 13. Hemispherical front end at v=0.25 m/s, pressure, velocity, and DFz=0.680 N

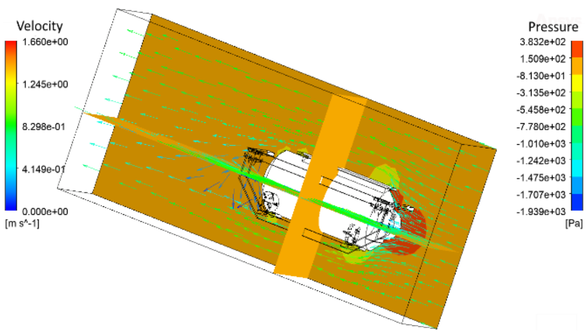

Fig. 14. Hemicylindrical front end at v=0.75 m/s, pressure, velocity, and DFz=43.46 N

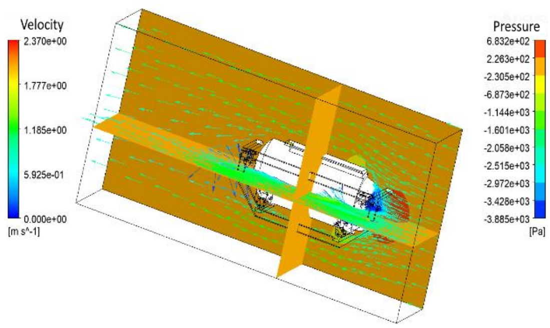

Fig. 15. Hemispherical front end at v=1 m/s, pressure, velocity, and DFz=65.408 N

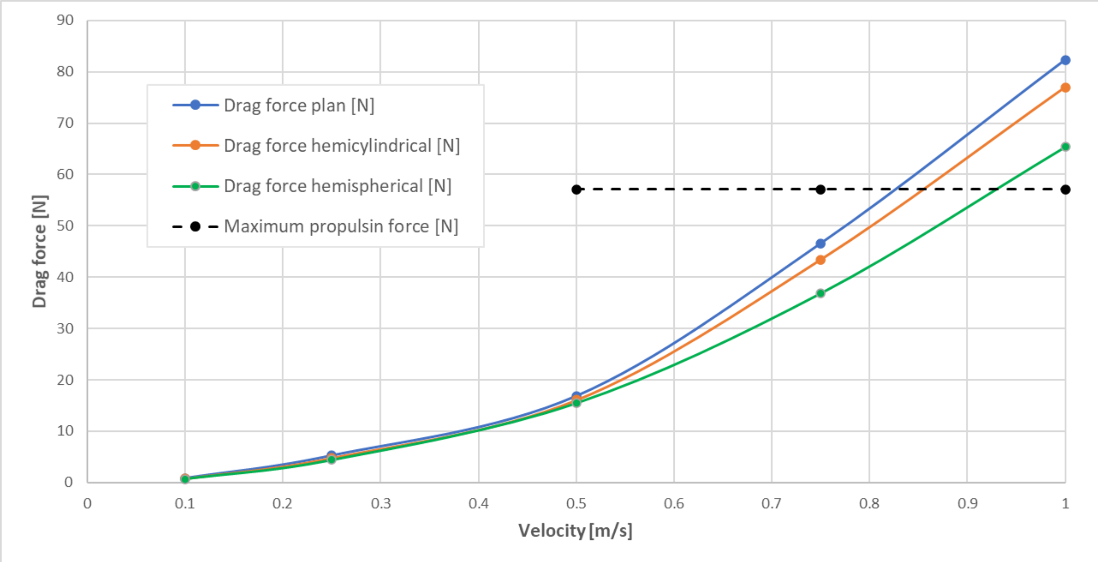

Fig. 16. Drag force versus velocity for 3 types of ROV front end

Figures 17, 18, and 19 show the 3 optimized models for which simulations were performed. The results are presented in Table 1 together with the performance indices, calculated as a percentage of the value variance, related to the correspondent value of the calibration model, shown in Figure 1, that are physically constructed and for which we have experimental measurements. This index shows the percentage of gain or loss made by the optimized model compared to the basic configuration

Figures 20-24 contain the most representative results obtained from the simulation. The centralized presentation of the achieving results was done in Table 1.

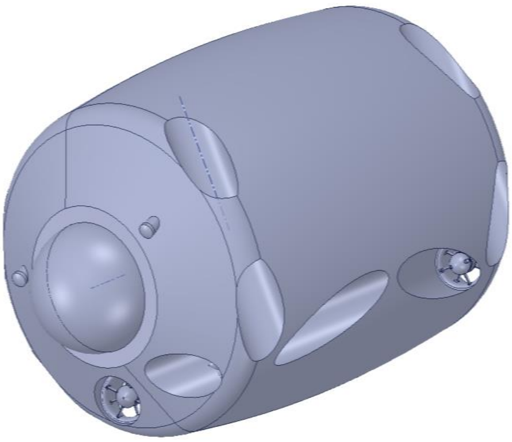

Fig. 17. ROV paraboloidal shape (ParaS)

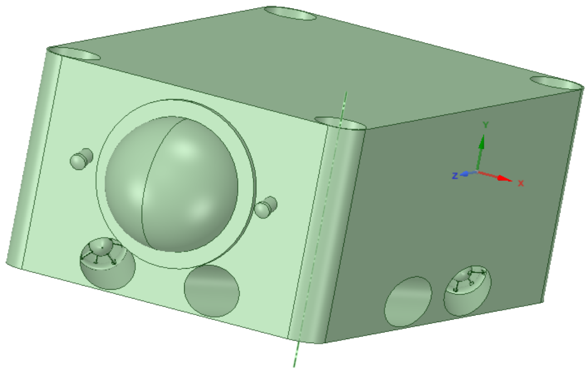

Fig. 18. ROV prismatic shape (PrisS)

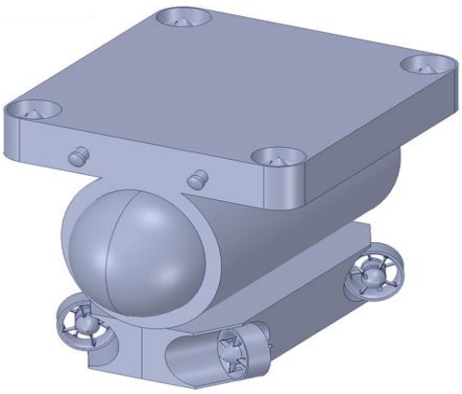

Fig. 19. ROV Composite shape (CompS)

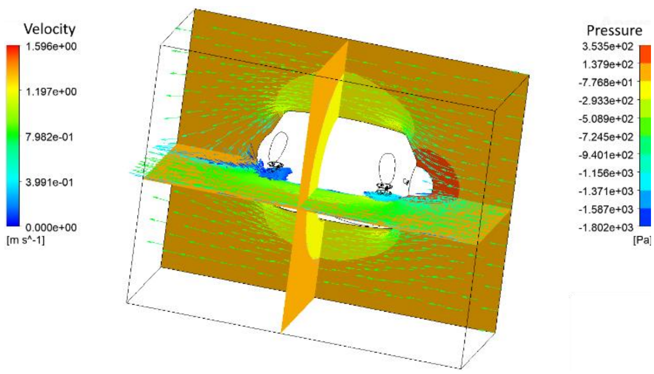

Fig. 20. ROV paraboloidal shape at v=0.75 m/s AHED, pressure, velocity and DFz=34.64 N

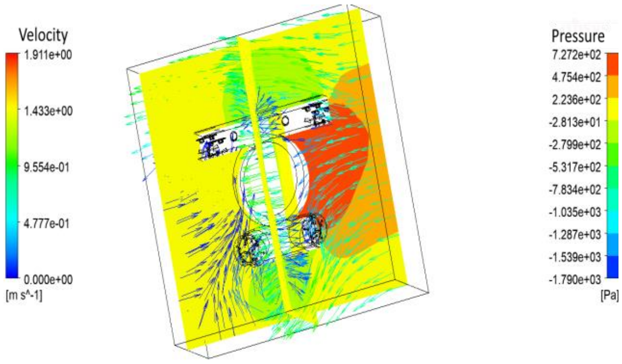

Fig. 21. Composite shape at v=0.75 m/s, PORT, pressure, velocity, and DFx=81.712N

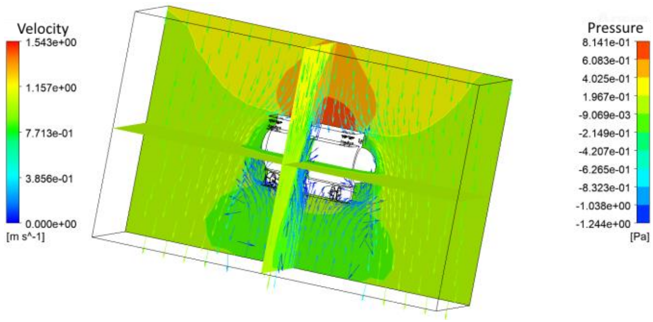

Fig. 22. Composite shape at v=0.75 m/s, UP, pressure, velocity and DFy=66.751 N

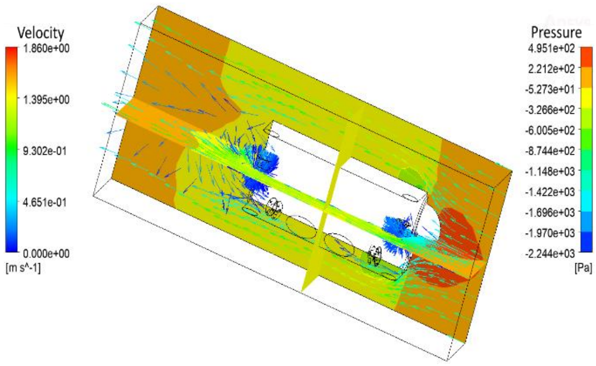

Fig. 23. ROV prismatic shape at v=0.75 m/s, AHED, pressure, velocity, and DFz=47.6 N

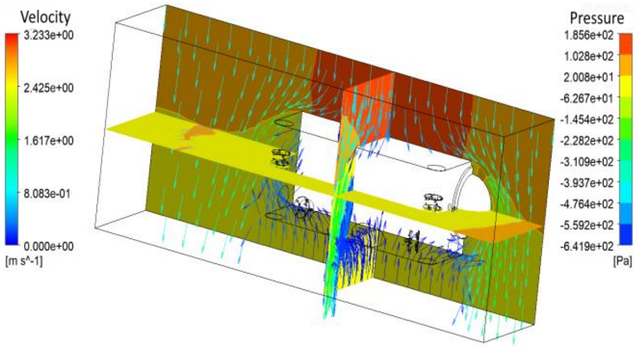

Fig. 24. ROV Prismatic shape at v=0.75 m/s, UP, pressure, velocity, and DFy=76.751 N

Table 1. Drag force for ROV models at 0.75 m/s speed

	Drag force AHEAD [N]/[%]	Drag force ASTERN [N]/[%]	Drag force PORT [N]/[%]	Drag force UP [N]/[%]	Drag force DOWN [N]/[%]
PlanF	46.6 / 0	48.6 / 0	**62.4 / 0**	72.8 / 0	**81.3 / 0**
SpheF	36.9 / 20.8	41.2 / 15.2	56.1/10.1	61.5 / 15.5	67.9 / 16.5
ParaS	34.6 / 25.8	35.1 / 27.8	49.2/21.2	51.2 / 29.7	53.6 / 34.1
PrisS	47.6 / -2.1	50.4 / -3.7	**67.3 / -7,9**	76.8 / -5.5	**88.4 / -8.7**
CompS	45.3 / 2.8	47.4/2.5	**91.7 / -30,9**	82.8 / -13.7	**79.1 / 2.7**
Propulsion max thrust	57.13	57.13	57.13	89.2	72.4

First of all, we can observe that the operating regime, established at a speed of 0.75 m/s, cannot be reached in all situations, with the available propulsion force (equation 9 and the last row in Table 1). The values are marked in bold in Table 1, and not influenced our analysis related to the hydrodynamical resistance, but is very important to take into account when designing the propulsion system.

The results obtained are in line with the expectations and results presented in other papers for similar underwater vehicles. As expected, the paraboloidal shape has the best nautical qualities and the weakest prismatic body, but it is worth noting that the differences between the frame structure and the closed body are so small. It is also true that the speed range is low (< 1 m/s) and for this reason, the influence of the hydrodynamic forces is lower, for high operating speed, the differences are expected to be greater. The effort required to achieve a closed structure ROV is much greater, much more difficult to maintain, and provides limited access to components.

The proposed hybrid body (CompS) has medium / low nautical qualities between those of the paraboloidal and the prismatic body, but it also offers major functional advantages, not to be neglected such as it is easy to make, offers a good cooling capability for the embedded components, offers easy access to all components for maintenance and has high stability in operation (maintaining direction) and positioning. For this reason, we are introducing this body in the analysis, many times the hydrodynamic characteristic of the ROV is surpassed by the functional ones.

The assessment of the nautical characteristics of the ROV did not take into account the oblique wire (tether), which plays a major role in the dynamics of wired-controlled underwater vehicles. From the literature [5] it is known that between 5 and 15% of the propulsion power is lost due to the wire, even if it has a null buoyancy. To have an estimation of the drag force given by the tether, a numerical simulation was performed (Figure 25 and 26). The conditions take in consideration ware a wire with a length of 1 m and a diameter of 10 mm positioned at 45 degrees in fluid current. For a cable whit a length of 50 m, frequently used in practice, in concordance with the data presented in Figure 26 the drag force is between 0.6 and 13.5 N which must be added to the body hydrodynamic force when designing the propulsion system.

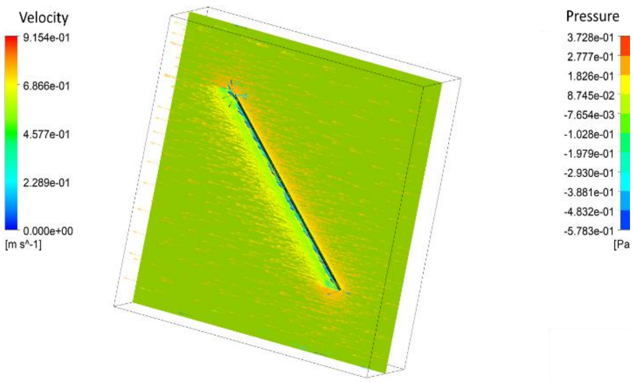

Fig. 25. Tether, 1 m at 0.75 m/s, velocity, pressure DFz=0,11 N

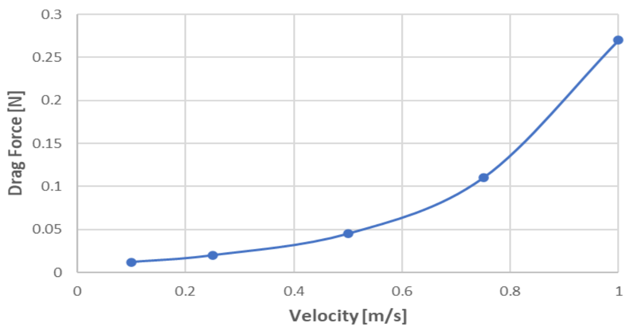

Fig. 26. Drag force versus velocity for 1 m length tether

6. CONCLUSIONS

The use of numerical simulation software to evaluate the nautical performance of ROVs and to optimize the body structure as seen in the presentation made are very useful and the results provided are in good agreement with reality. In particular, Ansys CFX is one of the best, well-known with verified results over time and a friendly and easy-to-use interface.

Designing an ROV is a major challenge, as it has to meet a large and varied number of requirements, especially in terms of manoeuvrability. For this reason, numerical simulation is essential. The optimal use of resources is of particular importance because that they are made in small and unique series production.

The optimization study carried out, as presented in the paper, highlighted using the numerical simulation, the strengths and weaknesses of each proposed model and allowed the adoption of solutions that meet as many requirements as possible.

To increase the accuracy of the simulation, more advanced models are needed that can run on accessible hardware configurations, especially for turbulent flow modelling. The simulations performed showed that at high speeds there are significant differences between the calculated and measured values.

For a complete ROV optimization, high-performance models are also needed to simulate the operation of the thrusters, but here things are even more difficult and the accuracy of the results obtained by numerical simulations is even lower.

7. ACKNOWLEDGMENTS

The authors are grateful for funding the publication of research from the project CNFIS-FDI-2022-0639 with title MCU- international landmark of excellence in maritime education and research.

8. REFERENCE

1. Zhang, D., Pan, G., Shi, Y., Wang, P., Chao, L., (2019). Investigation of the resistance characteristics of a multi-AUV system, *Applied Ocean Research*, 89, 59-70.
2. Caccia, M., Indiveri, G., Veruggio, G., (2000). *Modeling and identification of open-frame variable configuration unmanned underwater vehicles*, IEEE Journal of Oceanic Engineering, 25, 227-240.
3. Li, Z., Tao, J., Sun, H., Luo, Y., Ding, L., Deng, Z., (2017). *Hydrodynamic calculation and analysis of a complex-shaped underwater robot based on computational fluid dynamics and prototype test*, Advances in Mechanical Engineering, 9, 1-10.
4. Scurtu, I.C., Panaitescu, V.N., (2019). *Turbulent Flow Numerical Simulation for Unconventional Propulsion*, Revista de Chimie, 70(10), 3508-3511.
5. Christ, R.D., Wernli, R.L., (2014). *The ROV Manual*, 2nd Edition. (Butterworth-Heinemann, Oxford), 641-661.

Received: August 5, 2022 / Accepted: December 15, 2022 / Paper available online: December 20, 2022 © International Journal of Modern Manufacturing Technologies